ACS OMEGA

Article

Cite This: ACS Omega 2020, 5, 2603−2619

Hydrate Nucleation, Growth, and Induction

Bjørn Kvamme,*,† Solomon Aforkoghene Aromada,‡ Navid Saeidi,§ Thomas Hustache-Marmou,∥ and Petter Gjerstad‡

†State Key Laboratory of Oil and Gas Reservoir Geology and Exploitation, Southwest Petroleum University, Xindu Road No.8, Chengdu, Sichuan 610500, China

‡Department of Physics and Technology, University of Bergen, Allegaten 55, 5007 Bergen, Norway

§Department of Environmental Engineering, University of California Irvine, Henry Samueli School of Engineering, 4200 Engineering Gateway Building, Irvine, California 92697-3975, United States

∥Department of Fluid Mechanics, E.N.S.E.E.I.H.T Engineering School, 2 rue Charles Camichel, 31500 Toulouse, France

ABSTRACT: The first stage of any phase transition is a dynamic coupling of transport processes and thermodynamic changes. The free energy change of the phase transition must be negative and large enough to also overcome the penalty work needed for giving space to the new phase. The transition from an unstable situation over to a stable growth is called nucleation. Hydrate formation nucleation can occur along a variety of different routes. Heterogeneous formation on the interface between gas (or liquid) and water is the most commonly studied. A hydrate can also form homogeneously from dissolved hydrate formers in water, and the hydrate can nucleate toward mineral surfaces in natural sediments or a pipeline (rust). A hydrate particle's critical size is the particle size needed to enter a region of stable growth. These critical sizes and the associated nucleation times are nanoscale processes. The dynamics of the subsequent stable growth can be very slow due to transport limitations of hydrate-forming molecules and water across hydrate films. Induction times can be defined as the time needed to reach a visible hydrate. In the open literature, these induction times are frequently misinterpreted as nucleation times. Additional misunderstandings relate to the first and second laws of thermodynamics and the number of independent thermodynamics variables. It is not possible to reach thermodynamic equilibrium in systems where hydrates form in a pipeline or in sediments. Finally, there are common misconceptions that only one type of hydrate will form. In a non-equilibrium situation, several hydrates will form, depending on which phases the hydrate formers and water come from. In this paper, we utilize a simple nucleation theory to illustrate nucleation and growth of some simple hydrates in order to illustrate the non-equilibrium nature of hydrates and the fast nucleation times. To illustrate this, we apply thermodynamic conditions for a real pipeline transporting natural gas from Norway to Germany. This specific example also serves as a case for illustration of the possible impact of rusty pipeline surfaces in kicking out water from the gas. Specifically, we argue that the tolerance limit for water concentration according to current industrial hydrate risk practice might overestimate the tolerance by a factor of 20 as compared to tolerance concentration based on adsorption on rust.

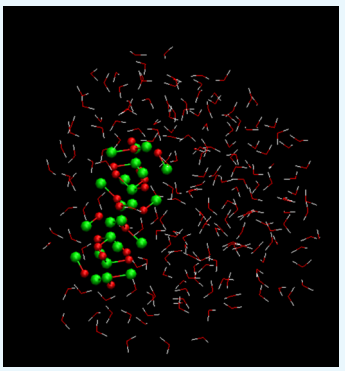

1. INTRODUCTION

The possible formation of hydrates is always a concern in natural gas processing and transport. During processing of natural gas, the conditions may be down to −22 ° C at around 70 bar, like in the processing of gas from the Troll offshore, Norway. However, temperatures may be as low as −70 °C in plants with significant amounts of components from ethane and higher hydrocarbons. Transport of natural gas in the North Sea is normally at temperatures higher than 0 ° C but typically below 6 °C. Pressures during transport can be very high but are normally below 300 bar. Common to all these situations is that the conditions are well within hydrate-forming conditions in terms of temperature and pressure. Also, since both temperature and pressure are always given locally by process control and/or hydrodynamic flow, the system can never reach thermodynamic equilibrium. Even for the simplest system of pure methane in contact with water, this is easy to verify by summing up all independent thermodynamic variables and subtracting conservation laws and conditions of equilibrium. This ends up with a maximum of one thermodynamic variable that can be specified for equilibrium to be achieved. This is of course well known to all since the methane equilibrium curve is always measured by keeping either P or T fixed and then monitoring the hydrate phase transition through slow variation of the other variable. A typical result comes out as plotted in Figure 1 below.

There is nothing unique about this figure, and there are numerous hydrate equilibrium codes worldwide that can calculate that curve. The reason for plotting it in the context of this paper is actually Figure 1b, which illustrates the chemical potential of water and the hydrate former as well as the free

Received: September 4, 2019
Accepted: December 6, 2019
Published: February 4, 2020

DOI: 10.1021/acsomega.9b02865
ACS Omega 2020, 5, 2603−2619

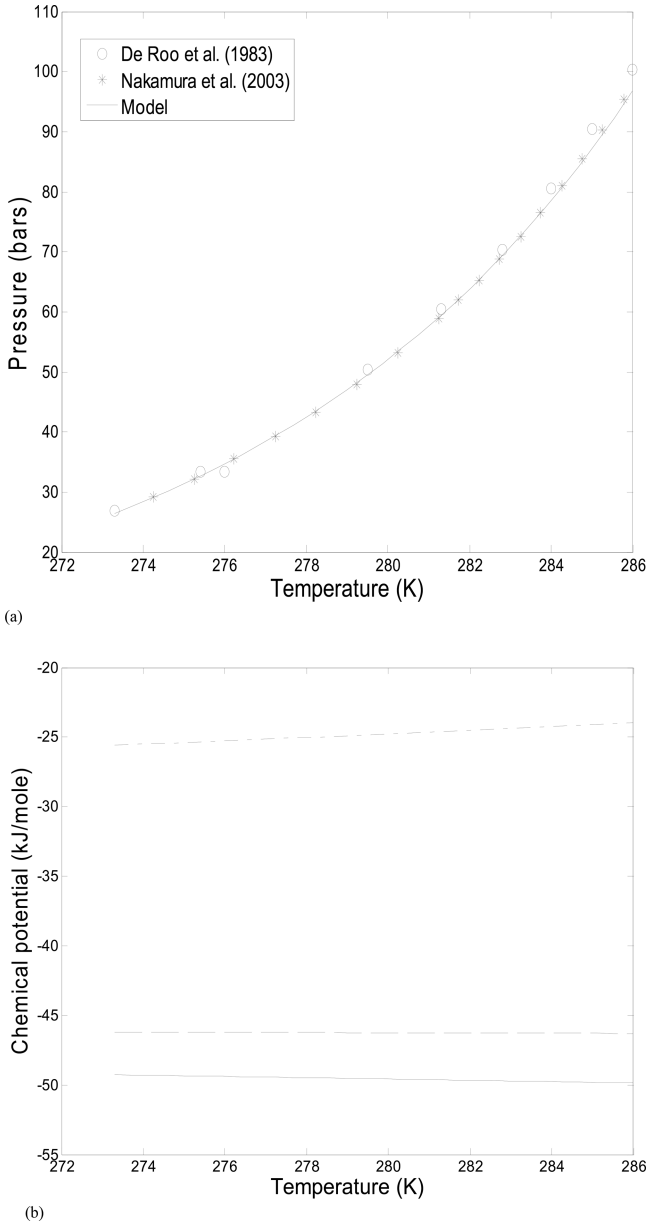

Figure 1. (a) Methane hydrate stability limits as a function of temperature and pressure. Solid curve is calculated; asterisks (*) are experimental data from Nakamura et al.,[1] and circles are experimental data from De Roo et al.[2] (b) Chemical potential for methane along the stability limit curve in panel (a) (dashed dotted line), chemical potential of water (solid line), and molar free energy (dashed line).

energy along the hydrate equilibrium curve. In general, in a non-equilibrium system, there is no rule that controls the chemical potential of each component to be equal across phase boundaries. On the contrary, it is minimum free energy under constraints of mass and energy conservation that controls the distribution of phases and phase compositions. Then, since chemical potentials of hydrate formers in various phases can be different, various routes to hydrates can result in different forms. In the simple system of a hydrate forming from water and methane, in the absence of solid surface effects, hydrate formation will then be on the interface as formulated in eq 1 below in terms of free energy change.

$$\Delta G^{(H_1)} = \left[x^{H_1}_{H_2O}(\mu^{H_1}_{H_2O}(T, P, \vec{x}^{H_1}) - \mu^{water}_{H_2O}(T, P, \vec{x})) + \sum_j x^{H_1}_j(\mu^{H_1}_j(T, P, \vec{x}^{H_1}) - \mu^{gas}_j(T, P, \vec{y}^{gas})) \right] \quad (1)$$

where μ denotes the chemical potential. Subscripts H_2O and j denote water and hydrate formers, respectively. The superscript H_1 is the hydrate phase, the superscript water is the liquid water phase, and the superscript gas is a separate hydrate former phase (gas, liquid, or supercritical). Mole fractions in the liquid are denoted as x, and mole fractions in the hydrate are denoted as x with a superscript H. y is the mole fraction in the separate hydrate former phase. For all of these mole fractions, the arrow on top means a vector of mole fractions. T and P are the temperature and pressure, respectively, and G is the molar free energy. The Δ symbol denotes a change in free energy. The hydrate formed through this particular route is denoted as H_1. This interface hydrate will rapidly grow to a solid membrane with low diffusivity for transporting gas molecules toward contact with water on the lower side of the hydrate film. Parallel to this mass transport-limited continuation of the H_1 hydrate, another hydrate can grow from the dissolved hydrate former in water.

$$\Delta G^{(H_2)} = \left[x^{H_2}_{H_2O}(\mu^{H_2}_{H_2O}(T, P, \vec{x}^{H_2}) - \mu^{water}_{H_2O}(T, P, \vec{x})) + \sum_j x^{H_2}_j(\mu^{H_2}_j(T, P, \vec{x}^{H_2}) - \mu^{water}_j(T, P, \vec{y})) \right] \quad (2)$$

The chemical potential of methane in various phases (gas, dissolved in water) is not necessarily the same in a non-equilibrium situation. In a non-equilibrium situation, the equilibrium conditions are replaced by local minimum free energy under constraints of mass conservation. The composition of this hydrate, H_2, will be different. This will be discussed in more detail later, but it is trivially given by the difference in cavity partition functions. For hydrate modeling tools using the fugacity of the hydrate-forming molecule times the Langmuir constant, this will appear through the difference in the fugacity of the hydrate former. In the formulations of Kvamme & Tanaka,[3] it appears through the chemical potential of the hydrate former in the cavity partition function.

Another possibility is that dissolved methane up-concentrates as it adsorbs toward the initial hydrate film H_1 and forms a hydrate heterogeneously there.

Theoretically, another possible route is from water dissolved in gas as given by eq 3 below.

$$\Delta G^{(H_3)} = \left[x^{H_3}_{H_2O}(\mu^{H_3}_{H_2O}(T, P, \vec{x}^{H_3}) - \mu^{gas}_{H_2O}(T, P, \vec{x}^{gas})) + \sum_j x^{H_3}_j(\mu^{H_3}_j(T, P, \vec{x}^{H_3}) - \mu^{gas}_j(T, P, \vec{y}^{gas})) \right] \quad (3)$$

Mass transport will be a substantial limitation for this particular route, and transporting hydrate formation heat through non-polar gas is also a substantial rate limitation. A limited amount of hydrate can, however, be formed from water

DOI: 10.1021/acsomega.9b02865
ACS Omega 2020, 5, 2603−2619

dissolved in gas if water condenses out on the already existing hydrate film. It is possible to estimate the theoretical amount of water that can condense out in this way by assuming a quasi-equilibrium situation. This calculation involves an estimation of how much water in the gas can be in quasi-equilibrium with hydrate water in H_1. A mass balance between the actual water content in gas and the quasi-equilibrium content of water in gas (with reference to water in H_1) will give a theoretical maximum hydrate film for water in gas.

Some solid surfaces, for instance, stainless steel, consist of neutral atoms and will not have any significant thermodynamic effect on the water structure. Pipelines for transport of hydrocarbons are typically rusty even before they are installed. Ordinary rust is a mixture of iron oxide, FeO, hematite, Fe_2O_3, and magnetite, Fe_3O_4. These three minerals will have different charges on the oxygens and irons and, correspondingly, different structuring effects on adsorbed water. The density of the first layer of adsorbed water on hematite may be three times higher than that of liquid water. The chemical potential of adsorbed water on hematite is substantially lower than that of liquid water. A typical industrial example is the impact of rusty pipeline walls on hydrate formation, as discussed in the next section for a relevant pipeline transporting natural gas from Norway to Germany.

However, even for the simple system of one hydrate former and water, we now end up with three different hydrates, so the number of degrees of freedom is −1 and the conditions of both temperature and pressure are highly over-determined in terms of the possibility for equilibrium.

Kinetic models for phase transitions are implicit dynamic couplings between mass transport of building blocks, associated heat transport, and thermodynamic control. This is also the case for the various routes to hydrate formation. In the classical nucleation theory, these couplings are very transparent. Multicomponent diffuse interface theory (MDIT)[4,5] reduces to the classical nucleation theory when the interface thickness approaches zero. Classical nucleation theory (CNT) can be expressed as

$$J = J_0 e^{-\beta \Delta G^{\text{Total}}} \tag{4}$$

where J_0 is the mass transport flux supplying building blocks for the hydrate growth. For the phase transition in eq 1, it will be the supply of methane to the interface growth. In eq 2, it will be the diffusion rate for dissolved methane to crystal growth from aqueous solution. Lastly, in eq 3, the rate-limiting mass transport is the supply of water by diffusion through gas. For eqs 1 and 2, transport through the structured water interface between the hydrate and surrounding liquid water will normally be the rate-limiting mass transport. The original classical nucleation theory is limited by a classical prefactor J_0 for single pure-component transport. As such, it is mainly limited to gas/liquid systems with very small or theoretically not significant interfaces.

The meaning of J_0 is still the same as in other systems, but it will be the limiting mass transport flux through the interface between the old phase and the new phases. In the case of hydrate nucleation and growth, a hydrate core will always be covered with water. For heterogeneous nucleation on the liquid water/gas interface, the capillary waves as well as capillary forces between hydrate water and liquid water will ensure that the hydrate core during nucleation is covered by liquid water. The actual rate-limiting transport in J_0 is therefore the transport of hydrate-forming molecules across an interface of gradually more structured water from the liquid side toward the hydrate side. The units of J_0 are mol/m^3 s for homogeneous hydrate formation in eqs 2 and 3 and mol/m^2 s for heterogeneous hydrate formation in eq 1. J has the same units as J_0. β is the inverse of the gas constant times the temperature, and ΔG^{Total} is the molar free energy change of the phase transition. This molar free energy consists of two contributions. The phase transition free energy as described by eqs 2 to 3, as examples, and the penalty work of pushing aside old phases. Since the molar densities of liquid water and hydrate are reasonably close, it is a fair approximation to multiply the molar free energy of the phase transition with the molar density of the hydrate times the volume of the hydrate core. The push work penalty term is simply the interface free energy times the surface area of the hydrate crystal. Lines below the symbols were used to indicate extensive properties (unit, Joules)

$$\underline{\Delta G}^{\text{Total}} = \underline{\Delta G}^{\text{Phase transition}} + \underline{\Delta G}^{\text{Pushwork}} \tag{5}$$

For the simplest possible geometry of a crystal, which is a sphere, with radius R, we then get

$$\underline{\Delta G}^{\text{Total}} = \frac{4}{3}\pi R^3 \rho_N^{\text{H}} \Delta G^{\text{Phase transition}} + 4\pi R^2 \gamma \tag{6}$$

where ρ_N^{H} is the molar density of the hydrate and γ is the interface free energy between the hydrate and surrounding phase. A small methane hydrate core growing on the surface of water is floating since the density of methane hydrate is lower than that of liquid water. Crystals below the critical size (and likely larger) will also be covered with water toward the gas side due to capillary forces and water adsorption.

The solution for maximum free energy and transition over to stable growth is found by differentiation of eq 6 with respect to R. The critical core size is indicated by the superscript * on R

$$R^* = -\frac{2\gamma}{\rho_N^{\text{H}} \Delta G^{\text{Phase transition}}} \tag{7}$$

For formation of the methane hydrate at various pressures inside the hydrate-forming regions, the critical hydrate core radius is typically between 18 and 22 Å for temperatures in the range of 274 and 278 K and pressures above 150 bar (see Figures 4 and 7 for examples of interface hydrate nucleation according to phase transition (eq 1)).

The implicit coupling to heat transport goes through the relationship between enthalpy changes and free energy changes. Equations 4 and 5 give a direct connection to the enthalpy change through the standard thermodynamic relationship

$$\frac{\partial \left[\frac{\Delta G^{\text{Total}}}{RT}\right]_{P,\vec{N}}}{\partial T} = -\left[\frac{\Delta H^{\text{Total}}}{RT^2}\right] \tag{8}$$

where ΔH^{Total} is the enthalpy change due to the phase transition and the associated push work penalty.

$$\dot{Q} \propto \Delta H^{\text{Total}} \tag{9}$$

Figure 2 illustrates the enthalpy of hydrate formation as calculated from the thermodynamic models for free energy based on residual thermodynamics and the use of eq 8. For details, see the studies of Kvamme[33] and Kvamme et al.[34]

Heat is mainly transported by conduction, convection, and radiation. Heat transport through liquid water and hydrate is 2 to 3 orders of magnitude faster than mass transport.[15] The

DOI: 10.1021/acsomega.9b02865
ACS Omega 2020, 5, 2603−2619

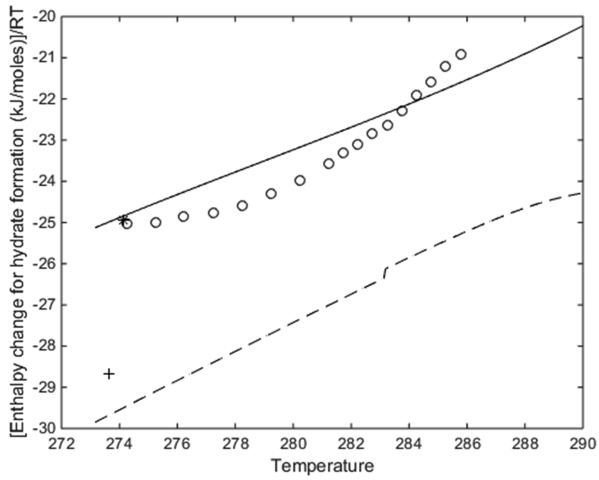

Figure 2. Calculated enthalpies of hydrate formation, in dimensionless units, along the pressure−temperature hydrate stability limit curve for CH_4. Solid line was obtained using eq 8. Circles are data from Nakamura et al.[1] for the CH_4 hydrate as calculated using a Clapeyron approach. The point (*) is a measured point from calorimetry experiments from Kang et al.[35] Dashed curve is the calculated enthalpy of hydrate formation from eq 8 for the CO_2 hydrate in dimensionless units. The plus symbol (+) is measured by calorimetry by Kang et al.[35]

details of eq 9 are not important in this work since the heat transport is not kinetically rate-limiting for the systems discussed here. The heat transport is of course proportional to the heat release (associated with the phase transitions), as expressed through eq 9 and coupled to eq 8 for the various hydrate formation routes in eqs 1−3. For phase transitions according to eqs 1 and 2, the heat transport is very fast and there is no rate-limiting factor in the phase transition kinetics. For eq 3, as mentioned above, there are limitations in mass transport due to low concentrations of water in the gas. However, the heat transport limitations of getting rid of the heat of hydrate formation given by eq 8 and various transport mechanisms through a non-polar gas in eq 8 are also critical.

This brings the discussion over to the title of the paper. There appears to be a lot of confusion in terms of the physical meaning of nucleation, growth, and induction. Equation 7 above defines the transition over to steady growth in classical nucleation theory. Onset of massive growth, as observed by induction times, is a function of many factors, but normally simple mass transport limitations. The purpose of this paper is to shed more light on this, and that is also why a simple theory is chosen. We use mostly more advanced concepts[6−8] in which the three components are much more implicitly integrated. However, classical nucleation theory provides a more visible distinction between the various contributions and serves better to illustrate that hydrate nucleation is really a nanoscale phenomenon and that the observed long induction times are a result of mainly mass transport limitations through hydrate films and/or a non-equilibrium situation that leads to dissociation of hydrates through contact with under-saturated phases.

The paper is organized as follows. Various routes to hydrate nucleation are discussed in the next section. This is followed by a section where a specific pipeline for transport of natural gas from Norway to Germany, Europipe II, is discussed in terms of hydrate risk evaluation based on the different routes to hydrate nucleation. The following section contains numerical calculations of the most relevant hydrate nucleation and growth paths. The final sections are a discussion of the results and the various stages of hydrate formation kinetics followed by our conclusions.

2. ROUTES TO HYDRATE FORMATION IF WATER DROPS OUT

Thermodynamically, three routes to hydrate formation based on the modes by which water is made available have been identified.[9−11] The first route is the dew-point route, which is the classical route currently considered and used for examining the risk of hydrate formation in industrial systems like during natural gas processing and pipeline transport. In this approach, the first step is calculation of the water dew-point concentration for the actual gas mixture at local conditions of pressure and temperature. If the actual water content in the gas is higher than the calculated dew-point concentration of water and the temperature and pressure are inside hydrate formation conditions, then there is a risk of hydrate formation. In this case, the gas is normally dried to below dew-point concentration.

Adding methanol, glycols, or other thermodynamic inhibitors at critical points for possible hydrate formation is frequently used. These thermodynamic inhibitors will change the hydrate stability region in the temperature−pressure projection of independent thermodynamic variables. Methanol will to a larger degree dissolve in gas as compared to glycols. This will shift the dew point, which is now a water/methanol dew point. Condensation of water/methanol droplets will therefore have a unique hydrate stability limit for the specific mole fraction of methanol in water that is shifted to higher pressures for hydrate formation. Injection of glycols are frequently preferred because glycols also have a corrosion-inhibiting effect and they are efficient in preventing hydrates from forming toward pipeline walls, as discussed below.

Water wetting solid surfaces gives rise to a second route toward hydrate formation. Stainless steel is neutral since it consists of uncharged atoms. However, normally, stainless steel is far too expensive for long transport limes. Plastic-covered pipelines are also neutral in terms of water adsorption. Any form for rust will be water-wetted due to the atomic charge distributions in the rust surface. Steel pipelines are normally stored outside before they are eventually transported and mounted together. The first rust that forms will normally be dominated by magnetite (Fe_3O_4) because of ready access to oxygen from air. Then, hematite (Fe_2O_3) and iron oxide (FeO)[9] will also form. Hematite is the thermodynamically most stable of these, and the other rust forms will gradually reorganize over to a dominating fraction of hematite. In this work, we therefore use hematite as a model for rust. The distribution of charged oxygens and irons in the hematite surface helps in making the surface very efficient for water adsorption. The average chemical potential for water adsorbed on hematite is very low[8,12,28] and far lower than the liquid water chemical potential. A hydrate can therefore not form from the first adsorbed water layers. The density of this first water layer is in the order of three times the liquid water density.[28] This is very typical for water adsorption on minerals, and experimental data are available for a variety of minerals like calcite and kaolinite, but we could not find experimental data for water adsorbed on hematite. Beyond the first layer, the density oscillates and the density minima outside of roughly five water molecules serve as traps for adsorbing hydrate formers in structured water.

Some minerals, like calcite and kaolinite, can adsorb CO_2 directly, but there is no evidence that CO_2 adsorbs directly on hematite, in competition with water. However, CO_2, CH_4, and

DOI: 10.1021/acsomega.9b02865
ACS Omega 2020, 5, 2603−2619

other small molecules that form gas can up-concentrate in structured water and/or condense on water films that have been generated by adsorption on hematite. From a mathematical point of view, an adsorbed water film represents an infinite number of phases because the density and structure of water change continuously. However, even if we only consider the adsorbed water as one phase, it is obvious that the number of independent thermodynamic variables is significantly higher than those obtained from conservation laws and conditions of equilibrium. Water drops out as a liquid or is adsorbed, and subsequent hydrate formation leads to systems that can never lead to equilibrium since the number of phases will never change in a continuous flow situation with a new supply of mass to all phases. In summary, the alternative route to hydrate formation involves water adsorbing on hematite, and the water layers beyond roughly five water molecules forming on the hematite surface can trap hydrate formers, or liquids like water further from the hematite surface make hydrate with hydrate formers from gas in the usual way like any liquid water phase. It should be kept in mind that the visible rust on pipelines that are being shipped out for mounting onto an offshore (or onshore) pipeline has rugged surfaces with visible peaks of rust heights. The relative adsorption surface per geometric pipeline surface is therefore huge on a molecular adsorption scale.

It is thermodynamically possible to form hydrates directly[8,12] from water dissolved in gas. The mass and heat transport limitation of this "direct route" is, however, substantial. Collecting in the order of 150 water molecules from a very dilute non-polar solution is a mass transport challenge. Re-structuring water molecules around non-polar solvent molecules releases heat. A second challenge is to get rid of the released heat. Heat transport through non-polar gas is extremely slow. It is much faster to redistribute the released heat through the structured water, and a re-dissociation of the hydrate cluster is a likely result.

If surface stresses from flow do not have any influence on the water/hydrocarbon system, then the hydrate formation occurs rapidly on the water/gas interface. Further transport of hydrate formers and water through the hydrate film will therefore be very slow, as discussed in more detail related to hydrate H_1 above. Formation of H_2 (see discussion above) will proceed until a quasi-equilibrium between water and methane in solution and the same components in hydrate occurs. In a flowing system with turbulent shear forces blocking the hydrate, films (membranes) will likely be broken and reformed continuously. The exceptions to this might be the shielded regions close to the pipeline walls. The rust in a pipeline will, as mentioned above, appear as a rugged surface in which peak heights are normally visible and, as such, which is several orders of magnitudes larger than the nanoscale size from a hydrate phase transition. In valleys between the high rust peaks, the effects of hydrodynamic stresses from outside flow decrease proportional to the distance from the rust peaks, toward the depth of the valleys. Also, unlike hydrate nucleation on a water/hydrate former interface, the hydrates formed toward hematite surfaces can only be bridged by structured water to the hematite surface. This opens up the potential of hematite surfaces to act as dynamic sites for nucleation of hydrates that will eventually detach from the surface and give room for new nucleation processes.

3. LIMITS OF WATER CONTENT IN HYDROCARBON FOR PIPELINE TRANSPORT

In this subsection, we have investigated the safety limit of water in gas pipeline systems based on the three routes of making water available as discussed in the previous section. Europipe II (EP II) is selected for this study because the temperature−pressure conditions are favorable for hydrate nucleation and growth. The EP II pipeline is around 660 km[13,14] long, out of which 627 km of the pipeline is offshore and goes through the Norwegian, Danish, and German parts of the North Sea. It is an export gas pipeline for transporting 65.9 mega standard cubic meters of gas per day[13,14] from the Kårstø processing plant in Norway to the Europipe receiving facilities (ERF) reception center at Dornum in Germany. This pipeline is laid on the seafloor of the North Sea where temperatures are generally low; they can be as low as −1 °C and seldom exceed +6 °C.[9,11,12] At the landfall in Germany, the temperature of the gas is expected to be as low as −5 °C.[13] The transport operation involves high pressures. The gas is sent from Norway at 190 bar, and it is received in Germany at 90 bar. These conditions of temperature and pressure are favorable for hydrate nucleation if water condenses out from the gas.

This practical industrial system is appropriate for our study of the limit of water content in natural gas to prevent water from dropping out to lead to hydrate nucleation. Therefore, our study covers a temperature range of −5 to +6 °C and a pressure range of 90 to 210 bar. The export natural gas is predominantly methane, so pure methane is assumed in this subsection. The usual criterion for avoiding hydrate formation in the pipeline is to make sure that water will not condense out from the gas. Molecular dynamics studies[28] indicate that the average chemical potential of adsorbed water on rust may be 3.4 kJ/mol lower than the chemical potential of liquid water. A more novel tolerance limit for water in natural gas will therefore be the maximum mole fraction of water in the hydrate former phase before water can drop out and adsorb on rust.

In classical hydrate risk evaluation, the formation of a separate liquid water phase through condensation will then be followed by hydrate formation if the local pressure and temperature are inside the hydrate stability curve. In the case of water adsorption on the pipeline walls, the hydrate will essentially form heterogeneously between water molecules slightly outside (roughly five water layers) of the rust surface where the water chemical potential is close to that of liquid water. In this region, there are still some density minima in the water structure that can dynamically trap hydrate formers and lower the energy barrier for the hydrate phase transition. Water droplets that follow the gas flow will be subjected to substantial surface stresses. The interface stress between the hydrate film covered by water droplets and surrounding flow can lead to hydrate film breakup. This might end up in a continuous chain of hydrate film breaking and heterogeneous formation of new hydrate films. As discussed above, hydrate films generated toward rust may be more shielded by roughness while at the same time having different dynamics in the formation and detachments of new hydrate nuclei toward rust. This roughness may be as large as that in visible hydrates (millimeter range) and creates pockets of shielded regions. In this case, dissolved natural gas in the water films on the solid surface can give rise to homogeneous hydrate formation as well as to two types of heterogeneous hydrate formations. The former is the initial hydrate film on the interface between natural gas and water, and the latter are the

DOI: 10.1021/acsomega.9b02865
ACS Omega 2020, 5, 2603−2619

subsequently heterogeneous hydrate formation from dissolved methane and water from below. Even though both water and methane come from the same liquid water phase, the real hydrate formation toward the initial hydrate film utilizes water, which is structured by the hydrate.

The results of our study of the Europipe II range of conditions are presented in Figures 3−5 and Table 1. The trends for the maximum amount of water allowable in the gas system without the risk of liquid water dropping out and/or hydrate formation for the three different routes to hydrate nucleation are the same. The difference is in absolute values. The maximum mole fraction of water that can be permitted without condensation of water or a hydrate forming directly from dissolved water in gas decreases with increasing pressures as can be observed in Figures 3 and 4. However, comparing values computed based on the different routes, the dew-point method estimates are in the order of 18 to 20 times higher than that of adsorption of water on hematite (rusty surfaces). This indicates that the presence of rust in pipelines makes it ∼20 times riskier for water to drop out through an adsorption process. The dew-point estimates are also 9 to 40% higher than those of the route of direct nucleation of hydrates where the highest difference occurs at the highest pressure and lowest temperature, while the least difference occurs at the lowest pressure and highest temperature (see Table 1). However, practically, hydrate nucleation through this direct route is highly unlikely as discussed above.

For defined pressure, temperature, and hydrocarbon composition, the water dew point is calculated by iteration of the mole fraction of water in the gas that will result in a water chemical potential in the gas equal to the liquid water chemical potential. Water adsorbed on hematite has a lower chemical potential than liquid water. Our estimates indicate that the chemical potential for water adsorbed on hematite may be 3.6 kJ/mol lower than the chemical potential for liquid water at 278 K. The mole fraction of water in the hydrocarbon phase before adsorption is solved in the same way as the dew point but now using the water chemical potential on hematite. For direct hydrate formation, the solution is using the water content in gas that results in zero for eq 3 above.

The pipeline gas may also contain more variety of hydrate formers. Some amount of higher hydrocarbons like ethane and propane might be present in Europipe II as given in Table 2, a report of composition data of export gas from Norway[16] published in 2012. This indicates that some amount of structure II hydrate are expected to form due to propane but this would be a very small amount as a consequence of the limited amount of propane in the reported gas mixture.[16] Therefore, different hydrates having different compositions of hydrate formers and different densities are expected in this situation. Hydrate risk analysis for this gas mixture was performed as done for the pure methane above. Figure 4a−c represents the results of the dew-point method, the method of adsorption of water onto rust, and the route of direct formation of hydrates from dissolved water in the gas mixtures, respectively. We can observe the impact of the heavier hydrocarbons on the upper limit of water allowable in the pipeline system by comparing Figure 3a−c with Figure 4a−c and Table 1 with Table 3. The maximum content of water permitted in the gas mixture reduces a bit by the presence of the higher hydrocarbons.

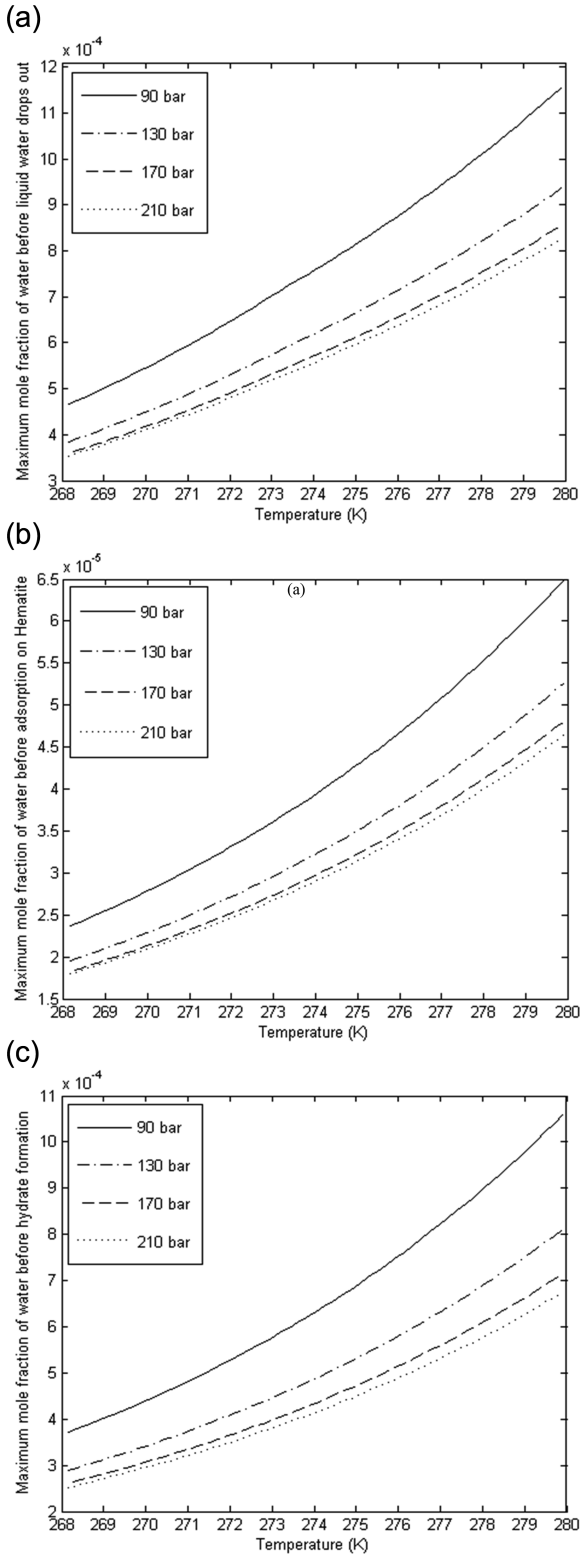

Figure 3. (a). Maximum water content before liquid water drops out of the transport gas. (b) Maximum water content before adsorption of water onto hematite. (c) Maximum water content before hydrate formation directly from water in the gas phase.

4. HYDRATE NUCLEATION AND HYDRATE GROWTH LIMITATIONS

Oxygens and hydrogens in hydrate water molecules are almost fixed, except from limited vibrations from energy minimum.[3]

DOI: 10.1021/acsomega.9b02865
ACS Omega 2020, 5, 2603−2619

Table 1. Maximum Water Content To Prevent Hydrate Formation during Transport of Export Gas [Pure Methane] from Kårstø in Norway to Dornum in Germany

		maximum allowable mole fraction at different temperatures and pressures			
temperature	route to hydrate formation	90 bar	130 bar	170 bar	210 bar
268 K	dew point	0.000466	0.000384	0.000359	0.000354
	hematite	0.000024	0.000020	0.000018	0.000018
	direct	0.000371	0.000289	0.000261	0.000252
274 K	dew point	0.000758	0.000620	0.000572	0.000558
	hematite	0.000040	0.000032	0.000030	0.000029
	direct	0.000632	0.000488	0.000435	0.000415
280 K	dew point	0.001155	0.000936	0.000855	0.000826
	hematite	0.000065	0.000053	0.000048	0.000046
	direct	0.001058	0.000811	0.000714	0.000674

Coulomb interactions between partial charges on oxygen and hydrogen are long-range. The phase transition occurs over a very thin interface of gradually changing water structure.[15,17,18] In earlier studies,[15,17,18] we used a 90% confidence interval for the distance from liquid water structure toward the hydrate water structure. This corresponds to a 1 nm interface thickness.

In classical nucleation theory (CNT), the prefactor is based on a single-molecule constant diffusional transport. Diffusional mass transport of two different types of molecules across the interface is involved in the hydrate formation dynamics. While the hydrate former is transported toward the hydrate core, the water closer to the hydrate core will expand and reform to cavity structures. Dynamically, this will be like a domino effect that leads to continuous renewal of the interface structure between the hydrate core and the liquid water outside. For mixtures, there will be diffusional transport of different hydrate formers, and in a dynamic situation, this can contribute in determining the hydrate composition. A hydrate core floating on liquid water can even be supplied with different hydrate formers from the gas side and the liquid water side (dissolved hydrate formers). Thermodynamically, CNT does not contain an interface thickness. However, the prefactor accounts for the transport across the interface to supply growth. In this work, we estimate diffusional transport and concentration gradients. These values are used in a Fick's type of approach for estimation of a realistic average value for J_0 in eq 4. It will still end up with a diffusional transport flux for every different size of a growing hydrate nucleus, and we can make use of sampled data from molecular dynamics simulations for concentration profiles across the interface from the liquid to hydrate interface.

The maximum hydrate filling will be below 100%, which would correspond to a methane hydrate mole fraction in the hydrate of 0.148. On the liquid side of the interface, it would be expected to be close to a value corresponding to the mole fraction of methane in water in equilibrium with the hydrate and lower than liquid water solubility. A second order fit of 0.14 for z equals to zero at the hydrate side and a liquid-side mole fraction 10 Å outside of that can be formulated as

$$\langle x_{CH_4}(z)\rangle = a_0 + a_1 z + a_2 z^2 \tag{10}$$

where the brackets denote average.

For a given stage of the growth, at size R, the average mole fraction of methane in the surrounding interface toward liquid water is estimated by

$$\langle x_{CH_4}(R)\rangle = \frac{2\pi \int_R^{R+10} [x_{CH_4}(z)] z^2 dz}{2\pi \int_R^{R+10} z^2 dz} \tag{11}$$

$$\langle x_{CH_4}(R)\rangle = \frac{2\pi \int_R^{R+10} [x_{CH_4}(z)] z^2 dz}{2\pi \int_R^{R+10} z^2 dz} = \frac{c_4 R^4 + c_3 R^3 + c_2 R^2 + c_1 R + c_0}{c_2^* R^2 + c_1^* R + c_0^*} \tag{12}$$

where

$$c_4 = 10a_2$$

$$c_3 = 200a_2 + 10a_1$$

$$c_2 = 2000a_2 + 150a_1 + 10a_0$$

$$c_1 = 10^4 a_2 + 1000a_1 + 100a_0$$

$$c_0 = 2000a_2 + 2500a_1 + \frac{1000}{3}a_0$$

$$c_2^* = 10$$

$$c_1^* = 100$$

$$c_0^* = \frac{1000}{3}$$

$$\frac{\partial x_{CH_4}(R)}{\partial R} = -\frac{(2c_2^* R + c_1^*)(c_4 R^4 + c_3 R^3 + c_2 R^2 + c_1 R + c_0)}{(c_2^* R^2 + c_1^* R + c_0^*)^2} + \frac{4c_4 R^3 + 3c_3 R^2 + 2c_2 R + c_1}{(c_2^* R^2 + c_1^* R + c_0^*)} \tag{13}$$

$$\frac{\partial^2 X_{CH_4}}{\partial R^2} = \frac{12c_4 R^2 + 6c_3 R + 2c_2}{c_2^* R^2 + c_1^* R + c_0^*} - \frac{2c_2^*(c_4 R^4 + c_3 R^3 + c_2 R^2 + c_1 R + c_0)}{(c_2^* R^2 + c_1^* R + c_0^*)^2} + \frac{2(2c_2^* R + c_1^*)^2 (c_4 R^4 + c_3 R^3 + c_2 R^2 + c_1 R + c_0)}{(c_2^* R^2 + c_1^* R + c_0^*)^3} - \frac{2(2c_2^* R + c_1^*)(4c_4 R^3 + 3c_3 R^2 + 2c_2 R + c_1)}{(c_2^* R^2 + c_1^* R + c_0^*)^2} \tag{14}$$

Diffusivity coefficient gradients for CH_4 across the interface between liquid water and the hydrate surface cannot be measured experimentally. Theoretical estimates for transport

DOI: 10.1021/acsomega.9b02865
ACS Omega 2020, 5, 2603−2619

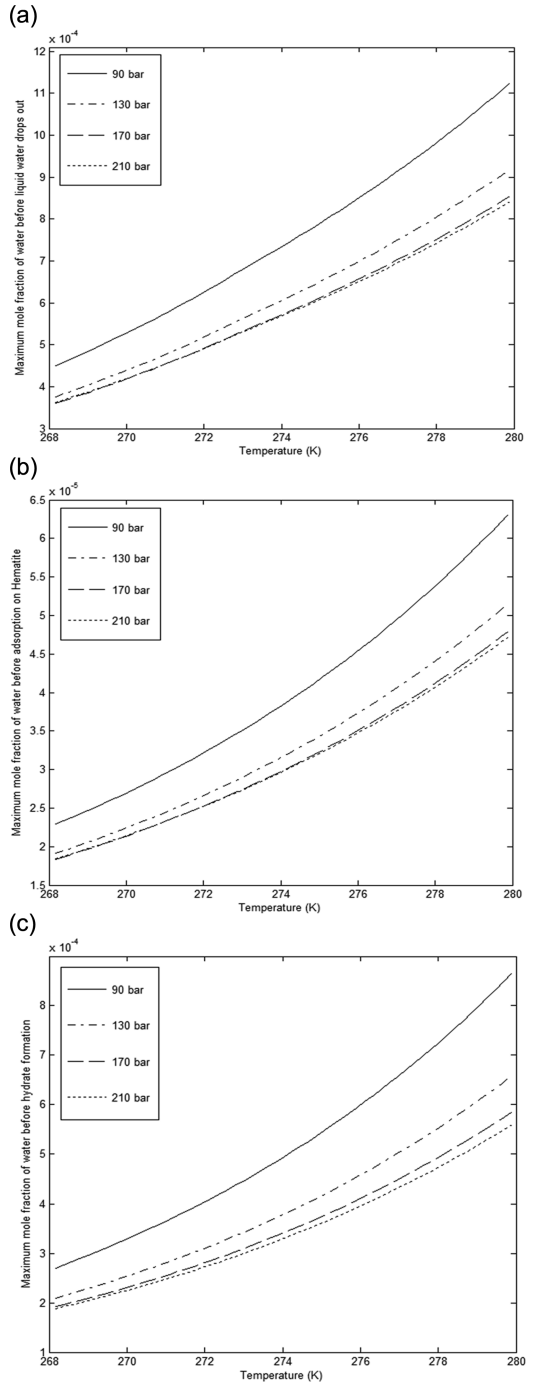

Figure 4. (a) Maximum water content before liquid water drops out of the export gas with a variety of hydrate formers. (b) Maximum water content before adsorption of water onto hematite (system with a variety of hydrate formers). (c) Maximum water content before hydrate formation directly from water in the gas phase (system with a variety of hydrate formers).

Table 2. Composition of Export Gas from Norway[16]

[mole fractions]				
methane	ethane	propane	*n*-butane	nitrogen
0.9203	0.0575	0.0131	0.0045	0.0046

of CH_4 through the solid hydrate are available from various open sources, but the relevance is questionable. Most estimated diffusivity coefficients are based on Monte Carlo studies for model systems of hydrate and guest molecules jumping between cavities.[19−21] The assumption is that a solid-state diffusion occurs when the hydrate guest jumps from an occupied cage to the neighboring empty cage through hexagonal or pentagonal faces of the water ring of structure I or II hydrate.[20−22] There is no verified mechanism involved in this cavity jumping mechanism. Molecular dynamics simulations[3] indicate that water molecules between filled and empty cavities have larger vibration amplitudes from minimum energy positions. These less stable boundary water molecules may be easier to be pushed temporarily out of position to let molecules pass from the filled cavity to the empty cavity.

The diffusivity coefficient of CH_4 at the surface of a hydrate is now denoted as D_H. The diffusivity coefficient of the liquid side of the interface is denoted as D_L. Since this is the 90% confidence interval of the interface structure, D_L should be somewhat lower than the diffusivity of CH_4 through "bulk" liquid water. D_H should be higher than the diffusivities through hydrates. Molecular dynamics studies[3] give substantially higher values for the diffusivity of CH_4 through hydrates than the Monte Carlo studies referenced above. As discussed above, we approximate the interface thickness to 10 Å and model the change in diffusion of CH_4 across the interface by a linear logarithmic approximation.

$$\ln D_{CH_4}(R, z) = \frac{\ln D_H - \ln D_L}{10}[(R + z) - R] + \ln D_L \tag{15}$$

For every radius R of a growing spherical hydrate particle, a volumetric average diffusivity in the interface layer surrounding the core is then estimated as

$$\langle D(R)\rangle = \frac{4\pi \int_R^{R+10} e^{\ln D_H - \ln D_L/10[(R+z)-R]+\ln D_L} z^2 dz}{4\pi \int_R^{R+10} z^2 dz}$$
$$= \frac{\int_R^{R+10} e^{b_0+b_1 z} z^2 dz}{10R^2 + 100R + \frac{1000}{3}} = \frac{R^2 d_0 + d_1}{b_1(d_2{*}R^2 + d_1{*}R + d_0{*})}$$
$$- \frac{Rd_2 + d_3}{b_1^2(d_2{*}R^2 + d_1{*}R + d_0{*})} + \frac{d_4}{b_1^3(d_2{*}R^2 + d_1{*}R + d_0{*})} \tag{16}$$

where $b_0 = \ln D_L$ and $b_1 = \frac{\ln D_H - \ln D_L}{10}$ and coefficients in eq 14 are given as follows

$$d_4 = 2e^{b_0+b_1R}(e^{10b_1} - 1)$$
$$d_3 = 20e^{b_0+b_1(R+10)}$$
$$d_2 = 2e^{b_0+b_1R}(e^{10b_1} - 1)$$
$$d_1 = (20R + 100)e^{b_0+b_1(R+10)}$$
$$d_0 = e^{b_0+b_1R}(e^{10b_1} - 1)$$
$$d_2{*} = 10$$
$$d_1{*} = 100$$
$$d_0{*} = 333.33$$

Then, we substitute X and D in Fick's second law equation

$$\rho\frac{\partial X_{CH_4}}{\partial t} = -D_{CH_4}(R)\rho\frac{\partial^2 X_{CH_4}}{\partial R^2} \tag{17}$$

DOI: 10.1021/acsomega.9b02865
ACS Omega 2020, 5, 2603−2619

Table 3. Maximum Water Content To Prevent Hydrate Formation during Transport of Export Gas with a Variety of Hydrate Formers

		maximum allowable mole fraction at different temperatures and pressures			
temperature	route to hydrate formation	90 bar	130 bar	170 bar	210 bar
268 K	dew point	0.000450	0.000376	0.000360	0.000362
	hematite	0.000023	0.000019	0.000018	0.000018
	direct	0.000270	0.000209	0.000192	0.000188
274 K	dew point	0.000736	0.000607	0.000573	0.000570
	hematite	0.000038	0.000032	0.000030	0.000030
	direct	0.000495	0.000379	0.000341	0.000330
280 K	dew point	0.001125	0.000919	0.000855	0.000841
	hematite	0.000063	0.000052	0.000048	0.000047
	direct	0.000866	0.000659	0.000586	0.000560

Since X is now only a function of R and t, we can substitute the integration variable X in eq 17 using

$$\frac{\partial X_{CH_4}}{\partial t} = \left(\frac{\partial X_{CH_4}}{\partial R}\right)\left(\frac{\partial R}{\partial t}\right) \tag{18}$$

which when inserted into eq 15 results in

$$\frac{\partial R}{\partial t} = -\frac{D_{CH_4}(R)\frac{\partial^2 X_{CH_4}}{\partial R^2}}{\frac{\partial X_{CH_4}}{\partial R}} \tag{19}$$

or

$$t(R) - t(R_0) = \int_{R_0}^{R} \frac{dR}{\left(-\frac{D_{CH_4}(R)\frac{\partial^2 X_{CH_4}}{\partial R^2}}{\frac{\partial X_{CH_4}}{\partial R}}\right)} \tag{20}$$

where R_0 is the starting size for the evaluation and the corresponding time appears on the left-hand side. Equation 19 is most conveniently integrated numerically.

The liquid-side concentration of methane in eq 10 is highly temperature- and pressure-dependent. It is beyond the scope of this work to do an extensive study of various liquid-side concentrations as a sensitivity analysis of surface concentration of methane. For this reason, we fix these parameters for a specific example. Parameters of $a_0 = 0.14$, $a_1 = -0.015$, and $a_2 = 2 \times 10^{-4}$ result in a mole fraction of methane equal to 0.14 at the hydrate surface. On the other side of the interface, 10 Å outside of the hydrate surface, the concentration of CH_4 is expected to be supersaturated relative to the solubility of CH_4 at specific temperature and pressure. For pipeline transport with pressure ranges in the order of 50 to 250 bar, a mole fraction of CH_4 equal to 0.01 10 Å outside the hydrate surface can be one example (see for instance Figures 6 and 7 below for bulk solubility as a function of temperatures and pressures).

4.1. Heterogeneous Hydrate Nucleation on Water/Gas Interface. There is only one degree of freedom in heterogeneous hydrate formation from liquid water and a single-component hydrate former phase. Equilibrium can therefore not be achieved when two independent thermodynamic variables are given. In any industrial situation of hydrate formation or any situation of hydrates in nature, both temperature and pressure are given locally. A first-order Taylor expansion from the stability limit can be written as

$$G^{H}_{\text{Non-equilibrium}}(T, P, \vec{x}) = G^{H,Eq.}(T^{Eq.}, P^{Eq.}, \vec{x}^{Eq.}) + \sum_r \left.\frac{\partial G^H}{\partial x_r}\right|_{P,T,x_{i\neq r}} (x_r - x_r^{Eq.}) + \left.\frac{\partial G^H}{\partial P}\right|_{T,\vec{x}} (P - P^{Eq.}) + \left.\frac{\partial G^H}{\partial T}\right|_{P,\vec{x}} (T - T^{Eq.}) \tag{21}$$

The reference state is the pressure−temperature stability limit curve for the actual gas composition. Any temperature on the equilibrium curve can be chosen freely. The last term in eq 21 therefore vanishes. The non-equilibrium free energy needed for eqs 5 and 6 can therefore be evaluated for eq 1 based on eq 21.

In Figure 5, we calculated the critical radius for hydrate formation from methane gas and liquid water on the interface according to eq 1. As in all other nucleation calculations, we have used a constant interface thickness between the hydrate and liquid water of 10 Å. We expect the nucleation to happen in the liquid water interface (10 Å). The applied value for interface free energy is 30×10^{-6} kJ/m^2,[23] and this value comes from experimental results for liquid water/ice. Except for very low driving forces, the critical nuclei radius is small.

4.2. Homogeneous Hydrate Nucleation from Dissolved Methane. The lowest limit of hydrate stability in terms of the surrounding water can be calculated from a quasi-equilibrium consideration. For the actual temperature and pressure, the chemical potentials of water and methane in the hydrate and in the solutions of water in contact are then the same. This will give a contour map of concentrations of methane in the surrounding water needed to keep the hydrate stable. The solubility of methane in water gives another contour map, which is calculated by the methane chemical potential in gas (or liquid or supercritical) being equal to the chemical potential of dissolved methane in water. Methane dissolved in water will be able to form a hydrate between the solubility of methane in liquid water and the minimum concentration for hydrate stability. Hydrate growth from methane dissolved in water is also dominated by heterogeneous hydrate formation. The reason is that methane dissolved in water will benefit from a heterogeneous growth toward the existing hydrate film. In order to calculate the kinetics of this nucleation process, we need the thermodynamic properties of methane adsorbed on the existing hydrate film and/or secondary adsorbed as trapped in water structures caused by the hydrate crystal. Separate studies are in progress using molecular dynamics simulations. The goal of these studies is to be able to quantify thermodynamic properties (chemical potentials and energies) as well as

DOI: 10.1021/acsomega.9b02865
ACS Omega 2020, 5, 2603−2619

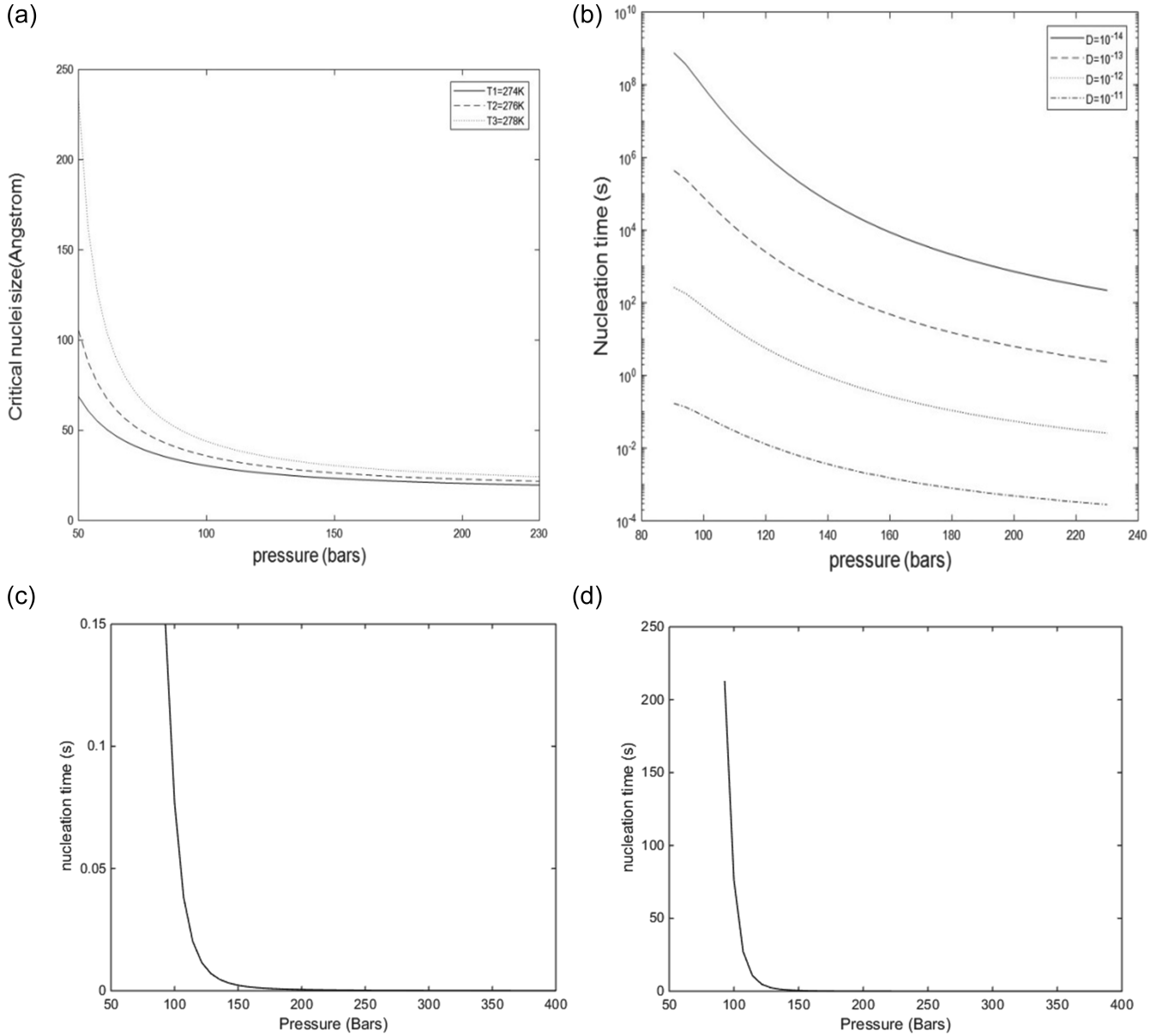

Figure 5. (a) Critical nuclei size for methane hydrate at three different temperatures for various supersaturations in pressure. Solid curve is for 274 K (equilibrium pressure of 28.4 bar). Dashed curve is for 276 K (equilibrium pressure of 34.7 bar). Dashed dotted curve is for 278 K (equilibrium pressure of 42.5 bar). All calculations were conducted using 30×10^{-6} kJ/m^2 for interface free energy between liquid water and the hydrate in eq 6. (b) Natural logarithm of nucleation time as a function of various pressures with different diffusion coefficients at a constant temperature of 274 K. (c) Nucleation time as a function of pressure for the CH_4 hydrate formed on the gas/water interface. Temperature is 274 K. The methane diffusivity on the hydrate side of the 10 Å-thick interface is 10^{-11} m^2/s. (d) Nucleation time as a function of pressure for the CH_4 hydrate formed on the gas/water interface. The methane diffusivity on the hydrate side of the 10 Å-thick interface is 10^{-12} m^2/s. Equilibrium pressure for 274 K is 28.4 bar.

diffusivities related to the structurally trapped methane. Homogeneous nucleation of the hydrate inside the water phase is also possible. This is the type of hydrate formation discussed in this work. As for the thermodynamic aspects related to the heterogeneous formations toward the hydrate film versus the homogeneous hydrate formation from solution, we may assume that the methane chemical potential toward the hydrate film is in quasi-equilibrium with the outside methane dissolved in water.

Guest chemical potentials in Figure 1b for methane in the gas phase as compared to chemical potentials of methane in solution in Figure 6b illustrate the variations in the resulting hydrate compositions through eqs 22−24 below. The associated differences in free energies for the various hydrates formed through different routes and "parent" phases (the phase where the molecule comes from) for the guest molecules are given by eq 25. The statistical mechanical equilibrium theory derived by Kvamme and Tanaka[3] differs from the classical methods in the sense that it gives the possibility of either a rigid lattice, like those used in other codes, or the use of a harmonic oscillator guest movement model in a molecular dynamics simulation for evaluation of the cavity partition functions. The canonical partition h_{ij} for a guest molecule j in cavity-type i evaluated by the latter option can be expressed as

$$h_{ij} = e^{-\beta[\mu_{ij} + \Delta g_{ij}]} \quad (22)$$

DOI: 10.1021/acsomega.9b02865
ACS Omega 2020, 5, 2603−2619

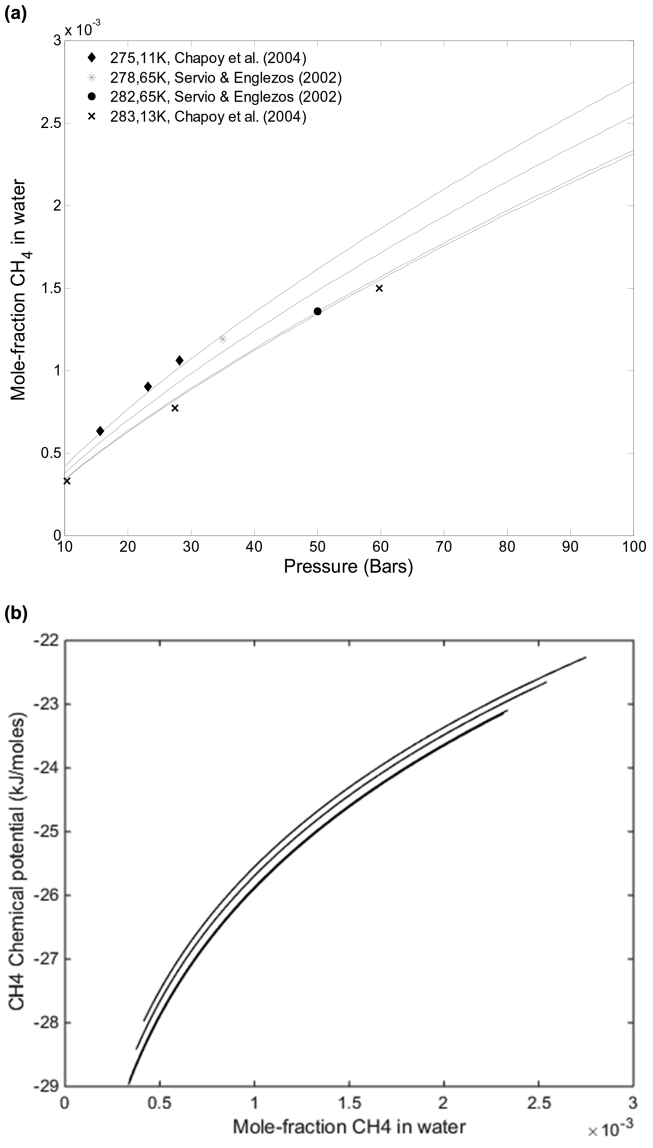

Figure 6. (a) Calculated solubility of CH_4 in water for four different temperatures. Top solid curve is for a temperature of 275.11 K, the next is for 278.65 K, then for 282.65 K, and the lowest solid curve is for 283.13 K. Experimental data from Chapoy et al.[24] are marked with solid diamonds and x marks, and experimental data from Servio and Englezos[25] are marked with asterisks and solid circles. (b) Chemical potential for CH_4 in aqueous solutions as a function of mole fraction along the solubility curves in panel (a). Top solid curve is for a temperature of 275.11 K, the next is for 278.65 K, then for 282.65 K, and the lowest solid curve is for 283.13 K.

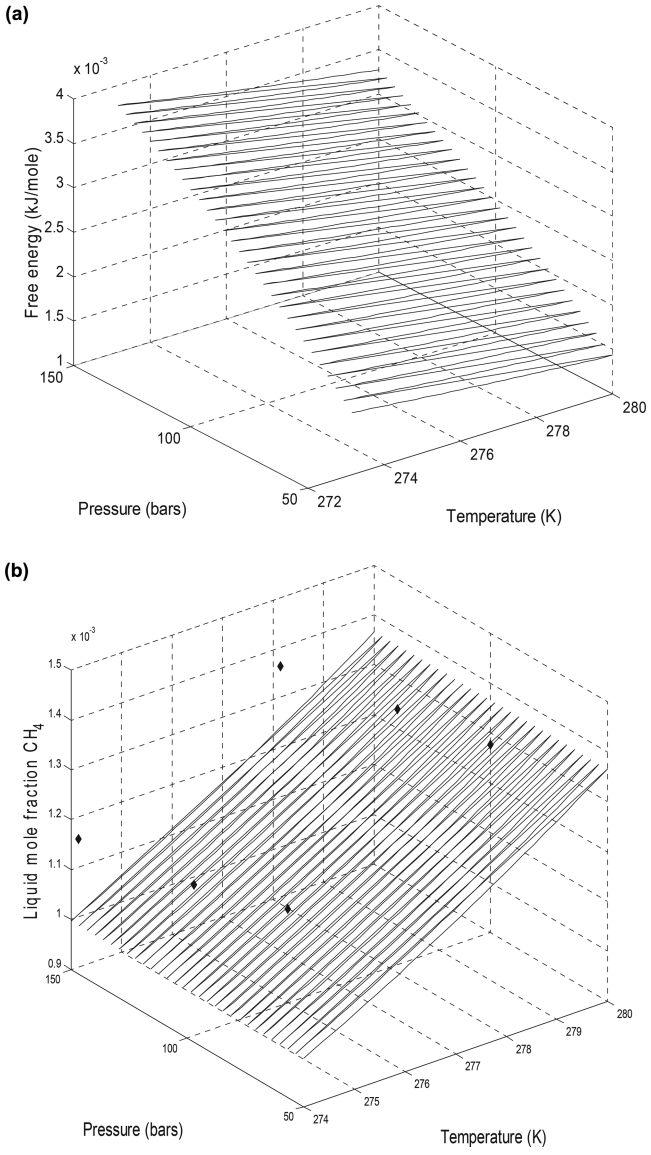

Figure 7. (a) Solubility of methane in water as a function of temperature and pressure. (b) Minimum methane in water for hydrate stability as a function of temperature and pressure. Solid line is estimated, and solid black dots are experimental data from Yang et al.[26]

In molar units, β is the inverse of the universal gas constant times the temperature. In molecular units, β is the inverse of Boltzmann's constant times the temperature. At equilibrium or at the stability limit for a non-equilibrium situation, the chemical potential of guest molecules j in hydrate cavity i is equal to the chemical potential of molecules j in the co-existing phase it comes from. For Figure 1, the hydrate former comes from a gas phase, while in Figure 6, it is the chemical potential for CH_4 in aqueous solution.

The corresponding filling fractions and mole fractions of methane in the hydrate are given by

$$\theta_{ij} = \frac{h_{ij}}{1 + \sum_j h_{ij}} \tag{23}$$

where θ_{ij} is the filling fraction of component j in cavity type i

$$x_j^{\mathrm{H}} = \frac{\theta_{\mathrm{large},j}\nu_{\mathrm{large}} + \theta_{\mathrm{small},j}\nu_{\mathrm{small}}}{1 + \theta_{\mathrm{large},j}\nu_{\mathrm{large}} + \theta_{\mathrm{small},j}\nu_{\mathrm{small}}} \tag{24}$$

where ν is the fraction of the cavity per water for the actual cavity type (indicated by subscripts). The corresponding mole fraction of water is then given by

$$x_{\mathrm{H_2O}}^{\mathrm{H}} = 1 - \sum_j x_j^{\mathrm{H}} \tag{25}$$

The associated hydrate free energy is then

$$G^{(\mathrm{H})} = x_{\mathrm{H_2O}}^{\mathrm{H}}\mu_{\mathrm{H_2O}}^{\mathrm{H}} + \sum_j x_j^{\mathrm{H}}\mu_j^{\mathrm{H}} \tag{26}$$

DOI: 10.1021/acsomega.9b02865
ACS Omega 2020, 5, 2603−2619

Superscript H refers to the hydrate. CH_4 chemical potentials for the heterogeneous formation from methane and liquid water in Figure 1 are different from CH_4 chemical potentials for homogeneous hydrate formation from water solutions in Figures 6b. From eq 26 and eqs 22−25, each of these hydrates will, by thermodynamic definition, be a unique phase because the composition, density, and free energy are different. Furthermore, as seen from Figure 6b, every different concentration of CH_4 between the solubility limit and hydrate stability limit will result in a unique hydrate. Mathematically, this means that an infinite number of hydrate phases can be formed from CH_4 in solution. The impact of the combined first and second laws of thermodynamics will, however, lead to reorganization of hydrates when the supply of new CH_4 is limited.

The experimental data referred to in the caption to Figure 6b are not directly comparable. Since there is free gas in the cell, there will be combinations of H_1 and H_2. Also, when CH_4 from solution is converted over to a hydrate, then new CH_4 will be dissolved from the free gas phase. It is therefore expected that the experimental values should be higher than what we calculated based on homogeneous hydrate formation from solution only. In view of this, the agreement is strikingly good.

Nucleation time decreases when the mole fraction of CH_4 in water increases, as illustrated in Figure 8. This is of course expected since the maximum thermodynamic driving force is when the concentration is at the solubility limit. For the concentration at the hydrate stability limit, the driving force is zero, and the closer we get to this limit, the higher the nucleation times become. Comparing different diffusivity coefficients shows that nucleation time is substantially faster for the example with a diffusivity of 10^{-11} m^2/s than the example with a diffusivity coefficient of 10^{-12} m^2/s. The expected range of limiting transport diffusivities based on comparison between experiments and results derived from phase field theory (PFT) modeling[7] is in agreement with this diffusivity coefficient.

4.3. Induction Times. As discussed in the previous sections, critical nucleation size is on the nanoscale order for the systems discussed in this work. As mentioned above, this is in accordance with the nano- to-mesoscale modeling published earlier from our research group[17] using phase field theory (PFT). Induction times, or times for "onset of massive growth", are frequently delayed by several factors. Mass transport limitations are frequently the most important.

As an example we may consider the reported result from an experiment in a stationary cell without stirring or other induced hydrodynamic effects.[9] The result is plotted in Figure 9 below. The reader is directed to ref 7 for more complete details on the experiment. The experimental cell is constructed by cutting a plastic cylinder of a diameter of 4 cm and length of 10 cm into two half cylinders. These two half cylinders are then squeezed together against a 4 mm-thick plastic spacer. The resulting empty space for fluids is then surrounded by a cooling medium. For monitoring, a magnetic resonance imaging system is utilized. For the applied frequencies, the hydrogen proton spin in hydrate water and methane hydrogen spin will be invisible. Liquid water spin is visible. Massive hydrate growth is then detected by the time when liquid water regions turn invisible due to hydrate conversion. Resolution of the experiment is limited to 300 μm. This number is different than the 100 μm resolution indicated by Kvamme et al.[7] and based on a more critical review of the experimental setup for this special experiment with a plastic container. The only thing that can be detected with this monitoring system is the transition over to rapid massive hydrate

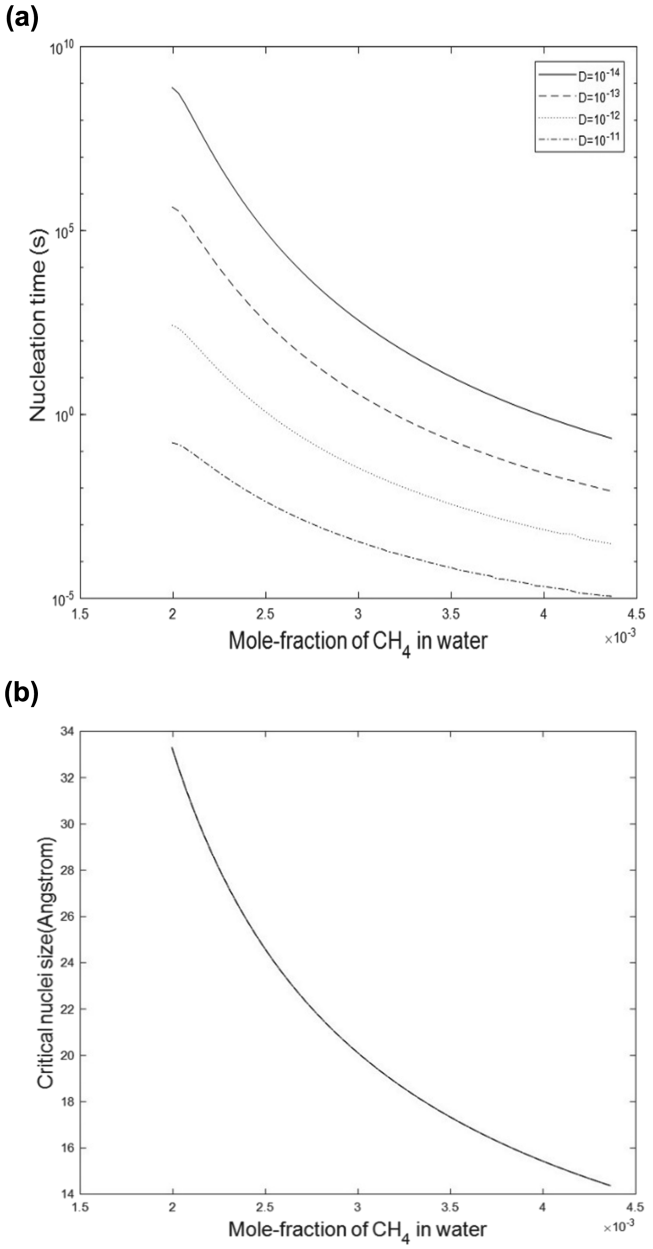

Figure 8. (a) Mole fraction of CH_4 dissolved in liquid water with respect to nucleation time at a temperature of 274 K and pressure of 200 bar with different diffusion coefficients. (b) Critical size as a function of mole fraction of CH_4 in water at constant temperature (274 K) and pressure (200 bar).

growth, as seen from Figure 9. The induction time ("time for onset of massive hydrate growth") was recorded to 100 h at conditions of 4 °C and a pressure of 1200 psig (84 bar). This level of induction time of 3.6×10^5 s is far beyond any possible value for nucleation times. Water and methane are both readily available on both sides of the interface between methane and water. Phase field theory modeling[7,15,27] reproduces the experimental observations with a diffusivity coefficient in the order of 10^{-12} m^2/s. For this particular setup, the plastic walls are methane-wetted. Capillary migration of methane along the plastic wall is one reason for accumulation of methane that is in contact with water along the wall. Another reason for the onset of massive growth is the rearrangements of the initial hydrate film between the gas and liquid water. The combined first and

DOI: 10.1021/acsomega.9b02865
ACS Omega 2020, 5, 2603−2619

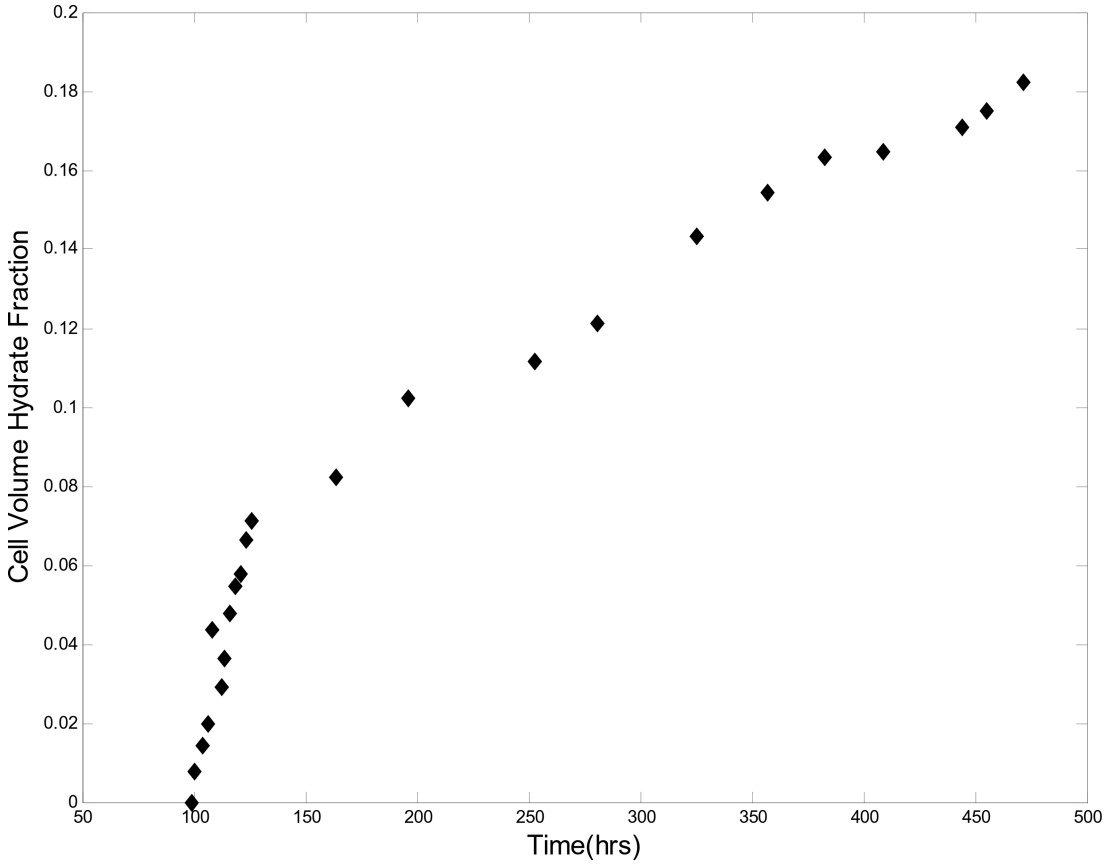

Figure 9. Experimental data for methane hydrate formation from water and methane at 1200 psia (83 bar) and 3 °C.[7]

second laws of thermodynamics will lead to rearrangements of the hydrate film. When there is a lack of new hydrate building blocks, then the most stable regions of the hydrate film will consume building blocks from less stable neighboring regions of the film. Eventually, this will lead to holes in the hydrate film. This latter effect is something that happens on all scales—from nano[7,15,17,27] to the visible scale as observed in experiments.[32]

5. DISCUSSION

Nucleation of hydrates can happen along a variety of routes. For natural gas hydrates in sediments or formation of hydrates in a rusty pipeline, the two most important routes are formation on the water/hydrate former phase and toward mineral surfaces. The relative importance of hydrate nucleation and growth from dissolved hydrate formers is related to the solubility of the hydrate former. In all cases, nucleation is a nanoscale phenomenon in time and space. Mass transport through a hydrate is very slow, and the time needed for a hydrate to grow to a visible size can be substantial, unless shear forces die to flow or other factors break the kinetically rate-limiting hydrate films. The time needed for a hydrate to reach a massive size to a visible hydrate is called the induction time. This time is frequently misinterpreted as nucleation time because the resolution of the monitoring device (magnetic resonance imaging, microscope, etc.) is not able to detect the presence of any hydrate.

Hydrates can never reach equilibrium in nature or industry. Even without the impact of solid surfaces, it is straightforward to verify that equilibrium of a single hydrate former and water distributed over three phases (water, hydrate, and hydrate former phases) is mathematically over-determined by one independent thermodynamic variable when temperature and pressure are both defined/given. Also, the situation does not improve if more hydrate formers are added since the first and second laws of thermodynamics will drive the phase transitions to a variety of different hydrate phases (different compositions). In a non-equilibrium system, the chemical potentials for a hydrate former in different phases are different because the first and second laws determine distribution of masses over the various possible phases. The result is that there are many different hydrates (different compositions and free energies). This variety is further enhanced for mixtures since the relative ability to adsorb on water is one part of the mass transport that brings water and hydrate formers in contact.

The most important routes to hydrate formation in sediments or industrial pipelines are via the water/hydrate former phase interface and toward mineral surfaces. The reason that the latter route is important is that the atomic charges on the mineral surface will dominate the structuring of water. The density of water in the first layer on a mineral surface can be three times the density of liquid water.[28] The associated chemical potential is substantially lower than the liquid water chemical potential.[8,28] The subsequent variations in water density as a function of distance from the mineral surface also involve regions of low water density that will be able to trap hydrate formers.[29−31]

Natural gas being transported in pipelines always contains water. It can be because of the equilibrium water saturation amount from the time the hydrocarbon system entered separation and processing units and finally ended up in a pipeline for transport. Normally, hydrodynamics will also distribute water into the hydrocarbon phases.

The low chemical potential of adsorbed water on rust implies that the rusty surface acts like a magnet for extracting water out

DOI: 10.1021/acsomega.9b02865
ACS Omega 2020, 5, 2603−2619

from the gas. Hydrate formation toward rusty pipeline walls can therefore be substantially more important than water condensing as droplets and the formed hydrate with gas. As discussed above, the hydrate is unable to stick to the rust surface. The hydrate formed toward rusty pipeline walls will also nucleate on hydrate films generated by dropped out water, roughly 6 water molecules distance (2 nm) from the surface of hematite.

For mixtures of various hydrate formers, the accessibility to hydrate formers on the water surface depends on the thermodynamic state for the various guest molecules and the attraction to the water surface. If we think about mixtures of CH_4 and CO_2 as one example, then CH_4 is supercritical in the liquid water hydrate range and does not have a tendency to condense. CO_2 is subcritical and has a favorable attraction to liquid water compared to CH_4. These aspects are illustrated by Kvamme[36] using a 2D adsorption theory. The average availability for hydrate formation on the liquid water surface and the associated average adsorption mole fraction on the liquid water surface are therefore very different from the gas mole fraction.

Another aspect that will also lead to a variety of different hydrates forming from CH_4 and CO_2 mixtures is the effect of the combined first and second laws of thermodynamics. The most stable hydrates will form first, under constraints of mass and heat transport. There are a number of common misunderstandings about hydrate stability. The stability limit in a temperature pressure projection is not the proper way to discuss stability. Since residual energy is used for all phases and all components, the molar free energy of each phase is the actual measure of the relative stability. In Figure 10a, we show a logarithmic plot of the temperature and pressure regions in which hydrates of CH_4 and CO_2 can form. For CO_2, the range of temperatures includes a phase transition to a lower density. In some published work, this transition is smoothened out. Still in other publications, it is discussed as a discontinuity.

However, the most important misunderstanding is in the discussion of stability in which it is frequently argued that the CH_4 hydrate is more stable above a certain temperature. This is not the case. If we plot the free energies of the two hydrates along the hydrate formation curves in Figure 10a, we can compare directly the stability of the two hydrates in Figure 10b,c. The stability limits of the CH_4 hydrate are compared to experimental data in Figure 1a, while those of the CO_2 hydrate are compared to experimental data elsewhere.[36,37] The free energy of the two hydrates in the three-dimensional plot in Figure 10b is hard to read in terms of specific numbers and only serves the purpose of showing the very different pressure dependencies for the two components after the temperature of the phase transition to higher density for CO_2. Figure 10c is easier to read and shows that the CO_2 hydrate is more stable than the CH_4 hydrate over the entire range of temperatures and pressures of the two $P-T$ stability curves in Figure 10a. These features are not directly visible in the old-fashion hydrate $P-T$ stability limit curves because they are based on semi-empirical fitting of the liquid water chemical potential minus the empty hydrate chemical potential.

In this work, we have utilized a numerically very simple theory, but it is still a theory with roots in physics as opposed to empirical fitting equations. The relative importance of the mass transport, the heat transport, and the thermodynamic control for each different system in consideration is easy to visualize. It is easy to implement as extensions of existing hydrate risk evaluation tools. This approach can save industries money in terms of chemical additives because there may be situations that

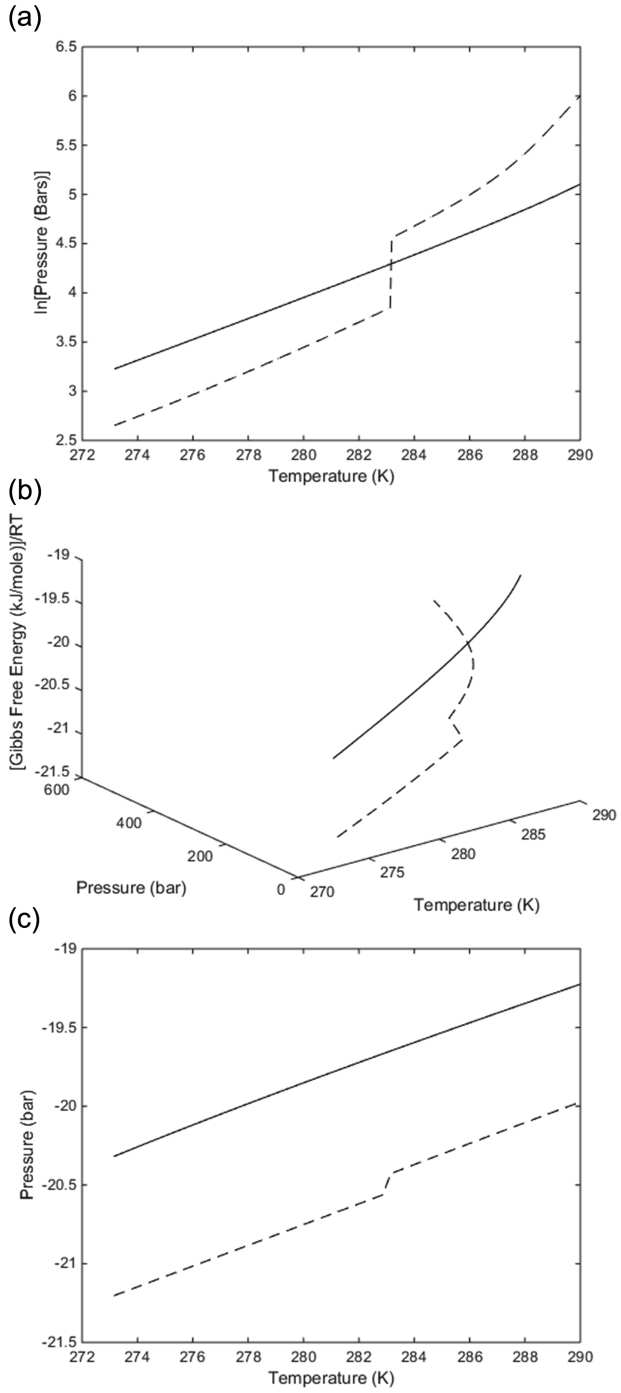

Figure 10. (a) Temperature−pressure stability limits for the CH_4 hydrate (solid) and CO_2 hydrate (dashed). (b) Dimensionless free energies of the CH_4 hydrate (solid line) and CO_2 hydrate (dashed line) along their corresponding hydrate stability limits in a pressure−temperature projection. (c) Dimensionless free energies of the CH_4 hydrate (solid line) and CO_2 hydrate (dashed line) along their corresponding hydrate stability limits in the temperature projection of the pressure−temperature space.

are in favor of hydrate formation from a pure thermodynamic analysis, while a more complete dynamic analysis may reveal that there are substantial kinetic limitations in mass transport or heat transport associated with the hydrate formation.

DOI: 10.1021/acsomega.9b02865
ACS Omega 2020, 5, 2603−2619

6. CONCLUSIONS

Misconceptions about hydrate nucleation times and hydrate induction times are frequently found in the open literature. In order to illustrate this, we have utilized a simple nucleation theory, CNT. Thermodynamic properties related to the phase transitions in this model are calculated using classical thermodynamics. Hydrate properties are derived from available results from molecular modeling in order to obtain a consistent and transparent reference level for all components in all phases. Except for situations of extremely low thermodynamic driving forces in terms of temperature and pressure, then the typical smallest hydrate cores (critical size) that enter growth regions are around 2 nm in radius. In the liquid water region, there is no experimental method that can detect such small hydrate cores and this is likely the reason that many researchers wrongly assume that there is no hydrate. The slow transport of hydrate formers through a hydrate film can cause substantial delays before hydrates of a visible size can be detected.

The influence of solid surfaces will often play a role in the transition to massive hydrate growth (induction time), but there are also several other factors related to thermodynamics. When there is no new material available for hydrate growth, the combined first and second laws will lead to a situation in which more stable regions of the hydrate film (regions of lower free energy) will consume neighboring regions of the hydrate film with higher free energy. Eventually, this can lead to holes in the hydrate film at a stage where massive hydrate growth is feasible due to the existing hydrate.

Minerals contain charged atoms that structure water to extreme densities compared to liquid water. Rust is a mix of various combinations of iron and oxygen, but the most stable is hematite. Pipelines for transporting hydrocarbons are rusty even from the point when they were welded together into a pipeline. The low chemical potential of water as adsorbed on hematite makes water substantially more favorable to adsorb on hematite rather than condensing out as liquid droplets during transport of hydrocarbon systems containing water. The first step in a hydrate risk evaluation analysis is a calculation of the water dew-point concentration for a local temperature and pressure in the pipeline. If this concentration is considered as the maximum amount of water to be permitted, then our calculations show that 18 to 20 times higher concentrations of water might be permitted as compared to a criterion based on the maximum concentration before adsorption on rust.

Another assumption that frequently occurs in the open literature is that only one hydrate structure forms. A variety of hydrates will form because industrial and natural systems of hydrates can never reach equilibrium. The chemical potentials of water and hydrate formers are therefore subjected to local free energy minimum as a function of mass and heat transport constraints. Cavity partition functions in the statistical mechanical theory for hydrates will therefore vary with local chemical potentials for guest molecules.

Hydrates forming from dissolved hydrate formers in water can come in many forms, depending on the concentration of the hydrate former versus solubility concentration and concentration at the limit of hydrate stability. Even though most of the focus in this paper has been on the CH_4 hydrate, we have also pointed out that comparison of hydrate formers need to be based on two levels of analysis. In a dynamic situation, subcritical components will have a stronger driving force to adsorb on liquid water than super critical components. Various components have their individual average attractions to liquid water prior to nucleation. In addition to these aspects, there will also be a selectivity based on gradients in free energy that directs the system toward the formation of most stable hydrates first. In real situations of mixtures of hydrate formers, many hydrates can form initially.

AUTHOR INFORMATION

Corresponding Author

*E-mail: kvamme_uib@outlook.com.

ORCID

Bjørn Kvamme: 0000-0003-3538-5409

Solomon Aforkoghene Aromada: 0000-0002-9054-4604

Notes

The authors declare no competing financial interest.

ACKNOWLEDGMENTS

Support from the University of California, Irvine and from Hyzen Energy is highly appreciated.

NOMENCLATURE

Å	Angstrom
δ	partial charge
P	pressure
P	number of phases (Gibbs phase rule)
T	temperature
T_R	actual temperature divided by the critical temperature
$T_{0,\,R}$	273 K divided by the actual temperature
R	universal gas constant
R	radius of hydrate core
R^*	critical radius for the hydrate core
ρ_N^{H}	molar density of hydrate
γ	interface free energy
γ_i	activity coefficient of a component
γ_i^{∞}	activity of a component at infinite dilution
μ	chemical potential
μ_i^{H}	chemical potential of component i in the hydrate cavity
μ_i^{gas}	chemical potential of component i in the hydrate former phase
μ_i^{water}	chemical potential of component i in liquid/gas or solid water
$\mu_{\mathrm{H_2O}}^{\mathrm{Water}}$	chemical potential of water in liquid/gas or solid water
$\mu_{\mathrm{H_2O}}^{0,\,\mathrm{H}}$	chemical potential of water in an empty hydrate cavity
μ_i^{∞}	chemical potential of a component at infinite dilution
G_i^{Ψ}	Gibbs free energy of a component at phase ψ
ΔG	change in Gibbs free energy
$\Delta G^{\mathrm{Total}}$	total change in Gibbs free energy
$\Delta g_{ik}^{\mathrm{inc}}$	Impact on hydrate water from the inclusion of guest i in cavity k
H	hydrate
H	enthalpy
H_{ik}^{R}	residual enthalpy of a component inside the cavity
ΔH	change in enthalpy
ΔS	change in entropy
x_i^{H}	mole fraction of component i in the hydrate
x_{ik}^{H}	mole fraction of component i in cavity k
$x_{\mathrm{H_2O}}^{\mathrm{H}}$	mole fraction of water in the hydrate
y_i^{gas}	mole fraction of component i in the hydrate former phase
J	mass transport rate

DOI: 10.1021/acsomega.9b02865
ACS Omega 2020, 5, 2603−2619

J_0	mass transport flux
β	inverse of Boltzmann's constant multiplied with temperature
m	mass
c and c^{eq}	supersaturated and equilibrium concentration
C	number of components (Gibbs phase rule)
F	degree of freedom
A	surface area of a crystal
K	overall transfer coefficient
K_d	diffusion coefficient
K_r	reaction coefficient
K_B	Boltzmann's constant
U	internal energy
$U_{ik}^{residual}$	residual contribution of energy for the guest in the cavity
S	entropy
N_j^i	number of particles of component j in phase i
n	hydration/occupation number
$\Delta U or dU$	change in energy

REFERENCES

(1) Nakamura, T.; Makino, T.; Sugahara, T.; Ohgaki, K. Stability boundaries of gas hydrates helped by methane—structure-H hydrates of methylcyclohexane and cis-1, 2-dimethylcyclohexane. *Chem. Eng. Sci.* **2003**, *58*, 269−273.

(2) De Roo, J. L.; Peters, C. J.; Lichtenthaler, R. N.; Diepen, G. A. M. Occurrence of methane hydrate in saturated and unsaturated solutions of sodium chloride and water in dependence of temperature and pressure. *AIChE J.* **1983**, *29*, 651−657.

(3) Kvamme, B.; Tanaka, H. Thermodynamic stability of hydrates for ethane, ethylene, and carbon dioxide. *J. Phys. Chem.* **1995**, *99*, 7114−7119.

(4) Kvamme, B. Kinetics of Hydrate Formation from Nucleation Theory. *Int. J. Offshore Polar Eng.* **2002**, *12*.

(5) Kvamme, B. Droplets of Dry Ice and Cold Liquid CO2 for Self-Transport of CO2 to Large Depths. *Int. J. Offshore Polar Eng.* **2003**, *13*.

(6) Kvamme, B.; Qasim, M.; Baig, K.; Kivelä, P.-H.; Bauman, J. Hydrate phase transition kinetics from Phase Field Theory with implicit hydrodynamics and heat transport. *Int. J. Greenhouse Gas Control* **2014**, *29*, 263.

(7) Kvamme, B.; Graue, A.; Buanes, T.; Kuznetsova, T.; Ersland, G. Storage of CO_2 in natural gas hydrate reservoirs and the effect of hydrate as an extra sealing in cold aquifers. *Int. J. Greenhouse Gas Control* **2007**, *1*, 236−246.

(8) Kvamme, B.; Kuznetsova, T.; Kivelæ, P.-H.; Bauman, J. Can hydrate form in carbon dioxide from dissolved water? *Phys. Chem. Chem. Phys.* **2013**, *15*, 2063−2074.

(9) Kvamme, B.; Aromada, S. A. Risk of Hydrate Formation during the Processing and Transport of Troll Gas from the North Sea. *J. Chem. Eng. Data* **2017**, *62*, 2163−2177.

(10) Kvamme, B.; Aromada, S. A. Alternative Routes to Hydrate Formation during Processing and Transport of Natural Gas with a Significant Amount of CO_2: Sleipner Gas as a Case Study. *J. Chem. Eng. Data* **2018**, *63*, 832−844.

(11) Kvamme, B.; Kuznetsova, T.; Bauman, J. M.; Sjöblom, S.; Avinash Kulkarni, A. Hydrate Formation during Transport of Natural Gas Containing Water and Impurities. *J. Chem. Eng. Data* **2016**, *61*, 936−949.

(12) Aromada, S. A. New Concept for Evaluating the Risk of Hydrate Formation during Processing and Transport of Hydrocarbons. Master's Thesis, Department of Physics and Technology, University of Bergen: Norway, 2017.

(13) Schuchardt, D.; Krause, D.-G. G.; Kulp, D. *Environmental Impact Assessment Europipe II in Germany: Offshore and Onshore Section*; Bioconsult Schuchardt & Scholle: Bremen, Germany, 1998.

(14) Gassco. *Europipe II*. Available: http://www.gassco.no/hva-gjor-vi/ror-plattformer/europipe-II/ (Acessed on April 5, 2018).

(15) Svandal, A. Modeling hydrate phase transitions using mean-field approaches. Dissertation for the Degree Philosophiae Doctor (PhD), University of Bergen: 2006.

(16) Denys, F.; de Vries, W. *Gas Composition Transition Agency Report 2013*; Gas Composition Transition Agency: Assen, The Netherlands, 2013.

(17) Tegze, G.; Pusztai, T.; Tóth, G.; Gránásy, L.; Svandal, A.; Buanes, T.; Kuznetsova, T.; Kvamme, B. Multiscale approach to CO_2 hydrate formation in aqueous solution: Phase field theory and molecular dynamics. Nucleation and growth. *J. Chem. Phys.* **2006**, *124*, 234710.

(18) Svandal, A.; Kuznetsova, T.; Kvamme, B. Thermodynamic properties and phase transitions in the $H_2O/CO_2/CH_4$ system. *Fluid Phase Equilib.* **2006**, *246*, 177−184.

(19) Falenty, A.; Salamatin, A. N.; Kuhs, W. F. Kinetics of CO_2-hydrate formation from ice powders: Data summary and modeling extended to low temperatures. *J. Phys. Chem. C* **2013**, *117*, 8443−8457.

(20) Salamatin, A. N.; Falenty, A.; Hansen, T. C.; Kuhs, W. F. Guest migration revealed in CO_2 clathrate hydrates. *Energy Fuels* **2015**, *29*, 5681−5691.

(21) Peters, B.; Zimmermann, N. E. R.; Beckham, G. T.; Tester, J. W.; Trout, B. L. Path sampling calculation of methane diffusivity in natural gas hydrates from a water-vacancy assisted mechanism. *J. Am. Chem. Soc.* **2008**, *130*, 17342−17350.

(22) Davies, S. R.; Sloan, E. D.; Sum, A. K.; Koh, C. A. In situ studies of the mass transfer mechanism across a methane hydrate film using high-resolution confocal raman spectroscopy. *J. Phys. Chem. C* **2009**, *114*, 1173−1180.

(23) Tuckerman, M. E. *Statistical Mechanics: Theory and Molecular Simulation*; Oxford University Press: 2010.

(24) Chapoy, A.; Mohammadi, A. H.; Richon, D.; Tohidi, B. Gas solubility measurement and modeling for methane−water and methane−ethane−n-butane−water systems at low temperature conditions. *Fluid Phase Equilib.* **2004**, *220*, 111−119.

(25) Servio, P.; Englezos, P. Measurement of dissolved methane in water in equilibrium with its hydrate. *J. Chem. Eng. Data* **2002**, *47*, 87−90.

(26) Yang, S. O.; Cho, S. H.; Lee, H.; Lee, C. S. Measurement and prediction of phase equilibria for water+ methane in hydrate forming conditions. *Fluid Phase Equilib.* **2001**, *185*, 53−63.

(27) Buanes, T. Mean-field approaches applied to hydrate phase transition. Ph.D. Thesis, University of Bergen: 2006.

(28) Kvamme, B.; Kuznetsova, T.; Kivelæ, P.-H. Adsorption of water and carbon dioxide on hematite and consequences for possible hydrate formation. *Phys. Chem. Chem. Phys.* **2012**, *14*, 4410−4424.

(29) Austrheim, M. H. Evaluation of Methane and Water Structure at a Hematite Surface - A Hydrate Prevention Perspective. MSc Thesis, Department of Physics and Technology, University of Bergen: Norway, September 2017.

(30) Nesse Knarvik, A. B. Examination of water and methane structuring at a hematite surface in the presence of MEG. MSc Thesis, Department of Physics and Technology University of Bergen, Norway, September 2017.

(31) Mohammad, N. Heterogeneous Hydrate Nucleation on Calcite [1014] and Kaolinite [001] Surfaces: A Molecular Dynamics Simulation Study. Master's Thesis, Department of Physics and Technology University of Bergen: Norway, June 2016.

(32) Makogon, I. F.; Makogon, Y. F. *Hydrates of Hydrocarbons*; 1st Ed.; Penn Well: Tulsa, ISBN-0-87814-618-7, 1997, 189−197.

(33) Kvamme, B. Enthalpies of hydrate formation from hydrate formers dissolved in water. *Energies* **2019**, *12*, 1039.

(34) Kvamme, B.; Aromada, S. A.; Gjerstad, P. B. Consistent Enthalpies of the Hydrate Formation and Dissociation Using Residual Thermodynamics. *J. Chem. Eng. Data* **2019**, *64*, 3493−3504.

(35) Kang, S.-P.; Lee, H.; Ryu, B.-J. Enthalpies of Dissociation of Clathrate Hydrates of Carbon Dioxide, Nitrogen, (Carbon Dioxide + Nitrogen), and (Carbon Dioxide + Nitrogen + Tetrahydrofuran). *J. Chem.Thermodyn.* **2001**, *33*, 513−521.

DOI: 10.1021/acsomega.9b02865
ACS Omega 2020, 5, 2603−2619

(36) Kvamme, B. Thermodynamic limitations of the CO_2/N_2 mixture injected into CH_4 hydrate in the Ignik Sikumi field trial. *J. Chem. Eng. Data* **2016**, *61*, 1280−1295.
(37) Kvamme, B.; Aromada, S. A.; Saeidi, N. Heterogeneous and homogeneous hydrate nucleation in CO_2/water systems. *J. Cryst. Growth* **2019**, *522*, 160−174.

DOI: 10.1021/acsomega.9b02865
ACS Omega 2020, 5, 2603−2619